Physica Scripta

ACCEPTED MANUSCRIPT • OPEN ACCESS

Characterization of cascaded arc He plasma in a compact linear plasma device using voltammetry and optical emission spectroscopy

To cite this article before publication: Yong Wang *et al* 2024 *Phys. Scr.* in press https://doi.org/10.1088/1402-4896/ad4290

Characterization of cascaded arc He plasma in a compact linear plasma device using voltammetry and optical emission spectroscopy

Yong Wang[1*], Hai-shan Zhou[2*], Xue-chun Li[2], Hao-dong Liu[2], Yi-wen Zhu[2], Guang-nan Luo[2]

[1]Navigation College, Dalian Maritime University, Dalian 116026, China

[2]Institute of Plasma Physics, HFIPS, Chinese Academy of Sciences, Hefei 230031, China

* Corresponding author: yongwang@dlmu.edu.cn and haishanzhou@ipp.ac.cn

Abstract

Cascaded arc plasma has been widely applied in linear plasma devices (LPDs) to produce high flux plasma for the study of plasma-material interaction. In this work, cascaded arc He plasma produced in an LPD with a compact arrangement is investigated by voltammetry and optical emission spectroscopy (OES). The results show that the cathode potential increases with the discharge current while it firstly decreases and then increases as increasing the gas flow rate. A local reverse electric field is observed at low gas flow rates between two cascaded plates (i.e. floating electrodes) near the cathode. The OES' results reveal that as the gas flow rate increases, the intensity of He I lines increases and the electron excitation temperature (T_{exc}) decreases. As increasing the discharge current, the intensity of He lines exhibits various trends at different gas flow rates, showing a monotonic decline at 1.94 slm and a first increase followed by a reduction at 3.52 slm. The T_{exc} increases with the discharge current. These findings could preliminarily shed light on the properties of cascaded arc of He plasma in the compact LPD and aid in the optimization of the device to generate the high-flux divertor-relevant plasma.

Keyword: cascaded arc He plasma, electron excitation temperature, emission line, *V-I* characteristic, linear plasma device

1. Introduction

Under the bombardment of plasma with extreme ion flux (~10^{24} $m^{-2}s^{-1}$) and heat flux (~10 MWm^{-2}), the wall in the future fusion reactors will be seriously eroded, limiting the lifetime of wall components and affecting the purity of fusion plasma. Plasma-wall interaction (PWI) has been one of the most critical issues with respect to the performance, safety and availability of fusion reactors[1]. In the present fusion devices, PWI issues have been widely studied. However, the significant gaps for some crucial PWI factors between the present tokamaks and future fusion reactor, like ion fluxes and fluences at the strike point, temperature of the plasma-facing components, pose large difficulties to explore all physics of PWI.

The versatility of linear plasma devices (LPDs) provides the possibility to close these research gaps. LPDs can produce the long-pulse and steady-state plasma, allowing to continuously expose materials to gain the desired fluence. At present, some LPDs can generate the plasma with ion and heat fluxes expected in the ITER divertor [2-5]. Meanwhile, the LPDs offer good accessibility and compatibility for the diagnostics including plasma diagnosis and sample analysis to in-situ and real-time study PWI processes [6]. In addition, compared with tokamaks, the construction and operation costs of LPDs are significantly cost-effective. These features make the LPDs important experimental platforms to investigate PWI processes.

Various LPDs have been developed based on different plasma sources [7-11]. However, only the helicon wave plasma source [5] (Proto-MPEX) and cascaded arc plasma source (CAPS) (Magnum-PSI/Pilot-PSI/CIMPLE-PSI) [2-4] have been reported to produce the plasma with ion flux up to 10^{24} $m^{-2}s^{-1}$. In China, within the Comprehensive Research Facility for Fusion Technology (CRAFT) project, a large superconducting linear plasma testing facility based on CAPS will be built to address some key R&D issues of plasma-facing materials and components for China Fusion Engineering Test Reactor (CFETR) and the facility is expected produce the reactor-relevant plasma (ion flux > 10^{24} $m^{-2}s^{-1}$) with duration of more than 1000 s [12]. To test and optimize the plasma source, a compact LPD, as a forerunner of the CRAFT LPD, has been established [12, 13]. The device is characterized by a compact designment which enables to enhance the magnetic field at the moderate current, realizing the long-pulse operation. The Ar gas was initially utilized as the working gas and how the Ar plasma operates in the compact arrangement is revealed in the previous work [13]. Ar, however, is not the tokamak's primary working gas. He or hydrogen isotope gasses should be used as the working gas in the compact LPD. This requires to diagnose the He or hydrogen isotope plasmas for the full understanding of the properties of plasmas in compact LPD and the application in PWI.

In the context, the upstream plasma in the CAPS is diagnosed by voltammetry and the cathode potentials under different currents and gas flow rates are acquired. Based on the measurements, the plasma behaviors can be deduced in the CAPS which can be considered as a 'black box', that is, it is difficult to directly diagnose the plasma. The optical emission spectroscopy (OES) is employed to characterize the downstream plasma. The radiation emitted from the plasma is revealed, which relates to the kinetic mechanism of He atoms. In addition, one of the basic plasma parameters, i.e. electron temperature, is calculated by Boltzmann plot method. Based on these measurements, the properties of He plasma in the compact LPD can be revealed, which will help us to optimize the discharge conditions to achieve the divertor-relevant plasma. This work is organized as follows. In section 2, the experimental setup is briefly described. In section 3, the results are presented and discussed. The last gives a summary.

2. Experimental setup

Figure 1 shows the schematic of the compact LPD. A cascaded arc plasma source is utilized to generate the high-density plasma. The plasma source is mainly composed of a tungsten cathode, five copper cascaded plates as the floating electrodes, and a copper anode. The plasmas source is connected to a 100 kW DC power source and the voltages between the electrodes are measured by a multimeter (Fluke, 17B+). The plasma source is mounted on a compact vacuum chamber with the inner diameter of about 120 mm. The compact arrangement enables to reduce the inner size of magnets for enhancing the magnetic field. To mitigate the thermal deposition on the chamber wall, an actively water-cooled jacketed design is adopted. The chamber is evacuated using a Roots pump with a pumping speed of 4500 m^3h^{-1} backed by a mechanical pump of 630 m^3h^{-1}. The pump system maintains the vessel pressure at several Pa during discharge. Four conventional water-cooled solenoid magnets are utilized to produce high magnetic field to confine the plasma. To increase the plasma density as much as possible, the whole plasma source together with the vacuum chamber are enclosed by the magnets. Figure 2 presents the axial distribution of magnetic field at different coil currents. The magnetic field up to 1 T can be achieved in the device. In figure 2, the origin $z = 0$ is taken at the nozzle of anode. More details about the device can be found elsewhere [12, 13].

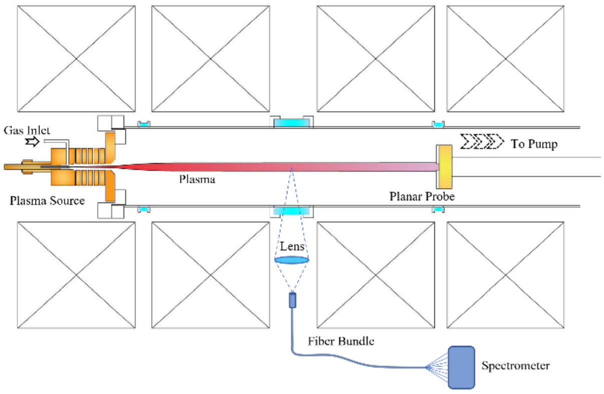

Figure 1. Schematic of the linear plasma device (not to scale.

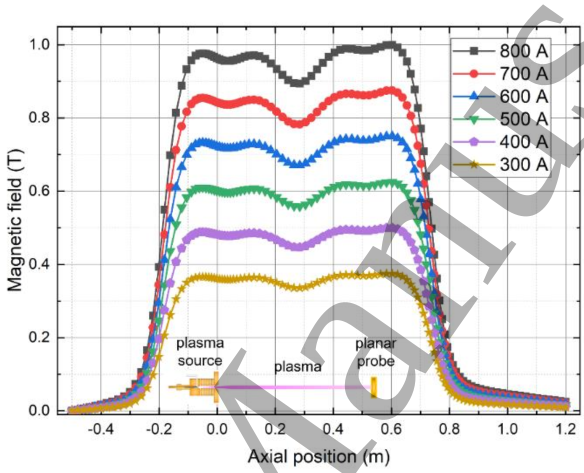

Figure 2. Axial distribution of the magnetic field in the SPARROW device at different coil currents. The origin $z = 0$ is taken at the nozzle of anode.

As a non-invasive and simple plasma diagnostic method, optical emission spectroscopy (OES) has been extensively applied in the linear plasma device. The excited species at upper level in plasma will emit the radiation when spontaneously relaxing to a lower level [14]. Based on the emitted radiation, the species in plasma can be distinguished. The information about basic plasma parameters, i.e. electron temperature (T_e) and electron density (n_e), can be determined via the intensity or line shape of the emitted lines. Hence, an OES system is built as well to gain insight into the optical properties of plasma as shown in figure 3. A plano-convex lens with focal length of 180 mm located at about 290 mm away from CAPS is employed to collect the emission light of downstream plasma. The light is focused onto a fiber bundle consisting of 8 fibers. The fiber bundle delivers the light to a muti-channel spectrometer (AvaSpec-Mini 4096CL, Avantes). The spectrometer is comprised of 8 modules and covers the spectral range of 200 to 960 nm.

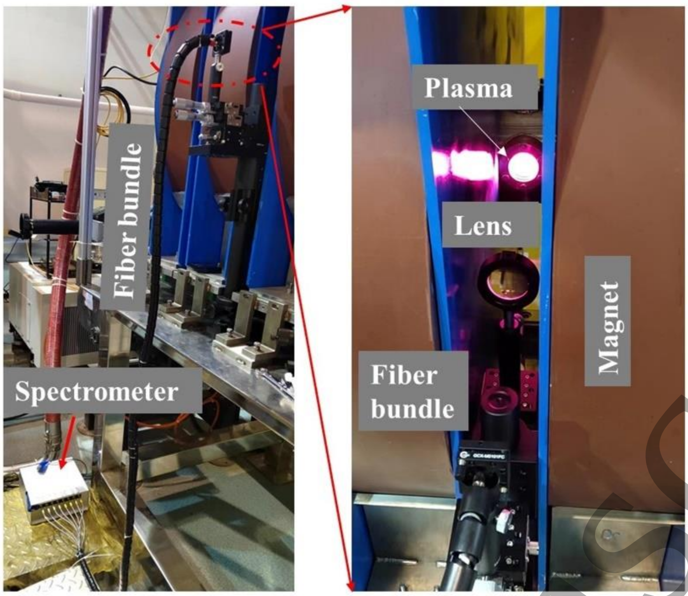

Figure 3. Photo of OES diagnosis for plasma in compact LPD.

3. Results and discussion

3.1 Characteristics of upstream plasma diagnosed by voltammetry

Figure 4(a) presents the results of *V-I* characteristics under gas flow rates of 3.52 slm and 0.88 slm at $B_{source} \approx 0.72$ T when the currents of four magnets is set as 600 A. Both the voltages increase as increasing the discharge current. The *V-I* characteristics were measured in other LPDs with CAPS as well. In SCU-PSI and DUT-PSI, the *V-I* characteristics with positive slope are also found[15, 16]. While the *V-I* characteristics in Pilot-PSI has a negative slope over the whole range of investigated currents at high gas flow and shows a shallow minimum at low gas flow[17]. The discrepancy should be ascribed to the different working gas and configuration of plasmas source. In Pilot-PSI, the working gas was H_2 and the CAPS contained three cathodes while in other devices He was the working gas and only single cathode was used.

The positive slope *V-I* characteristics could arise from the relationship $E = j/\sigma$ in which E is the electric field (representing the voltage), j the current density and σ the electrical conductivity [18]. In the arc column, σ increases with the arc temperature. However, due to the original large σ, the additional Joule heating is small, leading to a small increase in arc temperature, that is, σ increases lightly [19]. On the contrary, j increases linearly with the discharge current. Therefore, the electric field is enhanced that is, the voltage increases with discharge current.

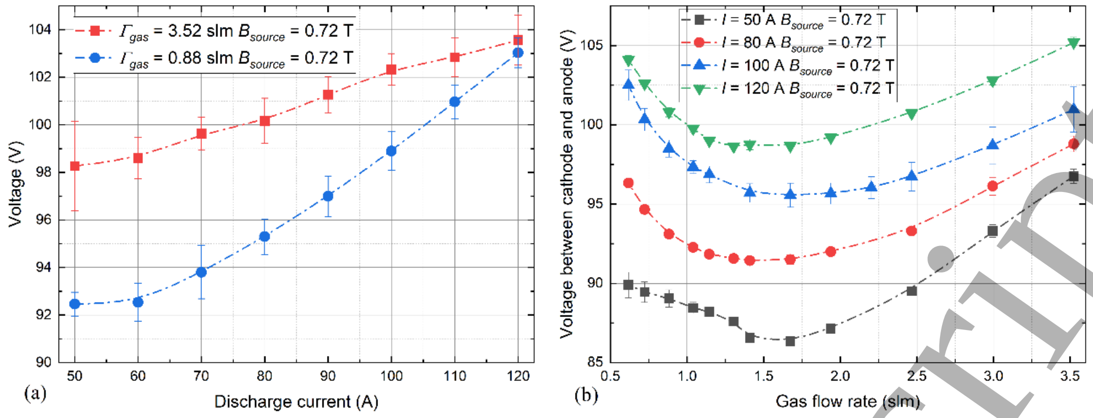

Figure 4. Voltage between cathode and anode as a function of (a) discharge current and (b) gas flow rate. Discharge conditions: (a) gas flow rates of 3.52 slm and 0.88 slm with B_{source} of 0.72 T, (b) discharge currents of 50 A, 80 A, 100 A and 120 A with B_{source} = 0.72 T.

The correlations between gas flow rate and arc voltage are shown in figure 4(b). The arc voltage firstly drops and then rises with the increase of gas flow rate. This is also different from the cathode potential in Pilot-PSI which increases as increasing the gas flow rate [17]. The drop in voltage should ascribe to the broadening of arc column. The increase of gas flow rate causes the collision between the particles. As a result, the radial cross-field transport of charged particles is enhanced and the arc column is broadened, leading to the decrease of arc voltage. In addition, Bora *et al* proposed that more thermionic electrons will be emitted from the cathode when the gas flow rate rises to lower the voltage drop near the cathode [20], which may also reduce the whole arc voltage. When the gas flow rate continues increasing, the arc column is surrounded by a cold boundary layer near the wall of electrodes and the arc temperature decreases by the convective heat. The drop in temperature induces the drop in σ which increases the arc voltage [21]. Moreover, the gas dynamic forces the arc roots to move more downstream to lengthen the arc column [18, 22], leading to an increase in arc voltage according to Nottingham equation [23]. Hence, the voltage increases at the high gas flow rate.

An interesting phenomenon is observed in our experiment. Figure 5 presents the voltages between anode and the first two cascaded plates, denoted as V_1 and V_2 respectively, versus gas flow rate. Normally, the 1st cascaded plate is closer to the cathode and V_1 should is greater than V_2. However, it is found that V_1 is smaller than V_2 at the low gas flow rate (<1.3 slm) at 100 A and 120 A and $V_1 \approx V_2$ at 50 A. This indicates that a local reverse electric field is formed between the first and second cascaded plates. At the high gas flow rate $V_1 > V_2$ again, suggesting that the reverse electric field vanishes.

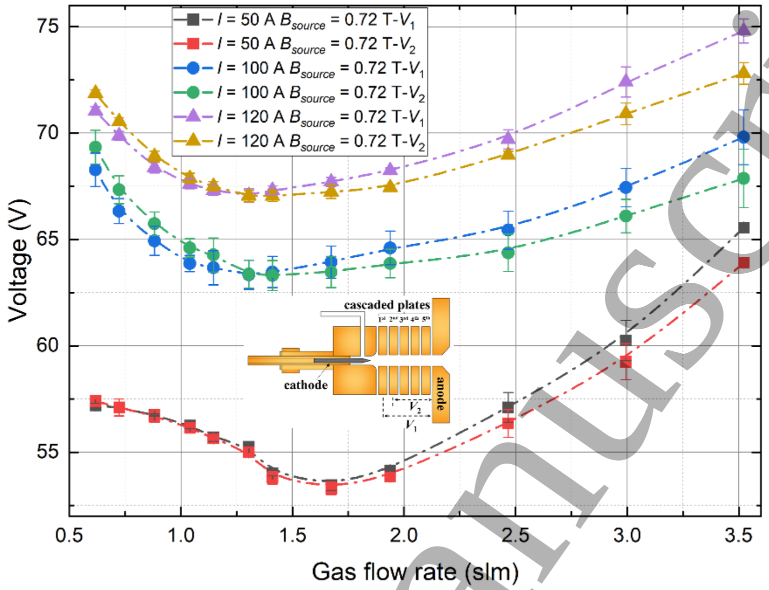

Figure 5. Comparison between voltage V_1 and V_2 with different gas flow rate at B_{source} = 0.72 T and current of 100 A and 120 A, respectively.

3.2 Characteristics of downstream plasma diagnosed by OES

3.2.1 Overview of the spectrum

The downstream plasma was diagnosed by OES. Figure 6 shows the typical spectra of He plasma with discharge currents of 50 A and 120 A at gas flow rate of 1.94 slm when the magnetic field at measured region of OES (B_{OES}) is about 0.67 T which is also generated by the currents of four magnets of 600 A, that is, distribution of magnetic field is identical to the case of B_{source} = 0.72 T as shown in figure 2. Here, B_{OES} is used to more accurately describe the discharge conditions. In general, the He atoms lines emitted by the levels with the small principal quantum number ($n \le 5$) are observed[24-27]. In our spectrum, the atomic line of 355.44 nm which is emitted by the level with n up to 10 are distinguished clearly at 120 A. Besides, the ionic line of 468.6 nm is also found, which does not be reported in the literature[24-27]. And this suggests that the electron density should be high in our plasma.

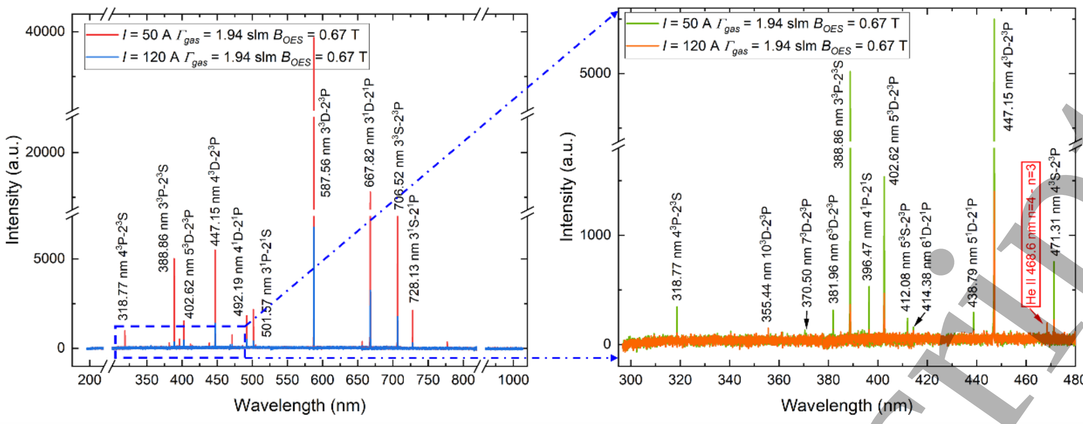

Figure 6. Typical spectra of cascaded arc He plasma at discharge currents of 50 A and 120 A, gas flow rate of 1.94 slm and B_{OES} of 0.67 T.

3.2.2 Behavior of the He atomic lines

Figure 7 shows the intensity of three typical He I lines with the wavelength of 587.6 nm, 667.8 nm and 706.5 nm as a function of gas flow rate at discharge current of 50 A and the magnetic field in OES region (B_{OES}) of 0.67 T. With the rise of gas flow rate, the intensity of these lines sharply becomes intense. This can be explained by the increase of population of the upper level, namely, 3^3D_2, 3^1D_2 and 3^3S_1, because the emission intensity of a spectral line is directly related to the population of upper excited state of transition.

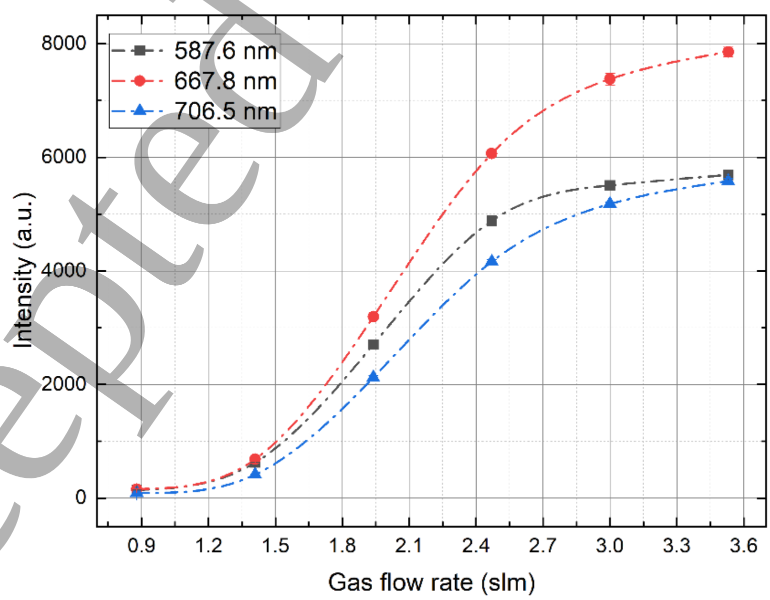

Figure 7. Intensity of He I lines (587.6 nm, 667.8 nm and 706.5 nm) as a function of the gas flow rate with discharge current of 50 A and B_{OES} = 0.67 T.

As for the downstream cascaded arc plasma, it belongs to recombing plasma and the recombination processes dominate the plasma [28-30]. The He atoms at excited states (He^*) can be produced via the recombination processes, including the radiative recombination and three-body recombination [27], as given by

$$\begin{gathered} \mathrm{He}^+ + e \rightarrow \mathrm{He}^* \\ k_1 = 6.67\times10^{-13} T_e^{-0.5}\ \ \mathrm{cm}^3\mathrm{s}^{-1}\ \ ^{[31]} \end{gathered} \tag{1}$$

$$\begin{gathered} \mathrm{He}^+ + 2e \rightarrow \mathrm{He}^* + e \\ k_2 = 7.8\times10^{-38}\left(T_e/T_g\right)^{-4.4}\ \mathrm{cm}^6\mathrm{s}^{-1}\ \ ^{[31]} \end{gathered} \tag{2}$$

where k is coefficient rate; T_e has unit eV and T_g has unit K.

Furthermore, it has been reported that the He atoms at the excited level of 3^3S_1 ($He^*(3^3S_1)$) emitting the line of 706.52 nm can be generated by the dissociative recombination of helium-molecular-ion (He_2^+) as given by reaction (3)[32-34]. He_2^+ is mainly formed via three-body ion conversion (reaction (4)) and associative ionization collisions with highly excited He atoms ($\mathrm{He}^*\left(n\geq3\right)$)[32-34]. 3^3D_2 and 3^1D_2 species emitting 587.6 nm and 667.8 nm should have similar production paths as these three lines show almost identical behavior [32, 34].

$$\begin{gathered} \mathrm{He}_2^+ + e \rightarrow \mathrm{He}^* + \mathrm{He} \\ k_3 = 7.12\times10^{-15}\left(T_e/T_g\right)^{-1.5}\ \mathrm{cm}^3\mathrm{s}^{-1}\ \ ^{[31]} \end{gathered} \tag{3}$$

$$\begin{gathered} \mathrm{He}^+ + 2\mathrm{He} \rightarrow \mathrm{He}_2^+ + \mathrm{He} \\ k_4 = 1.4\times10^{-31}\left(T_g/300\right)^{-0.6}\ \ \mathrm{cm}^6\mathrm{s}^{-1}\ \ ^{[31]} \end{gathered} \tag{4}$$

$$\begin{gathered} \mathrm{He}^*\left(n\geq3\right) + \mathrm{He} \rightarrow \mathrm{He}_2^+ + e \\ k_5 = 1.5\times10^{-11}\ \ \mathrm{cm}^3\mathrm{s}^{-1}\ \ ^{[35]} \end{gathered} \tag{5}$$

With the increase of gas flow rate, it has been found that the n_e increases[15, 16], which indicates that more populations of He^* can be produced by the recombination reactions (1) – (3), leading to an increase of corresponding spectral lines intensity.

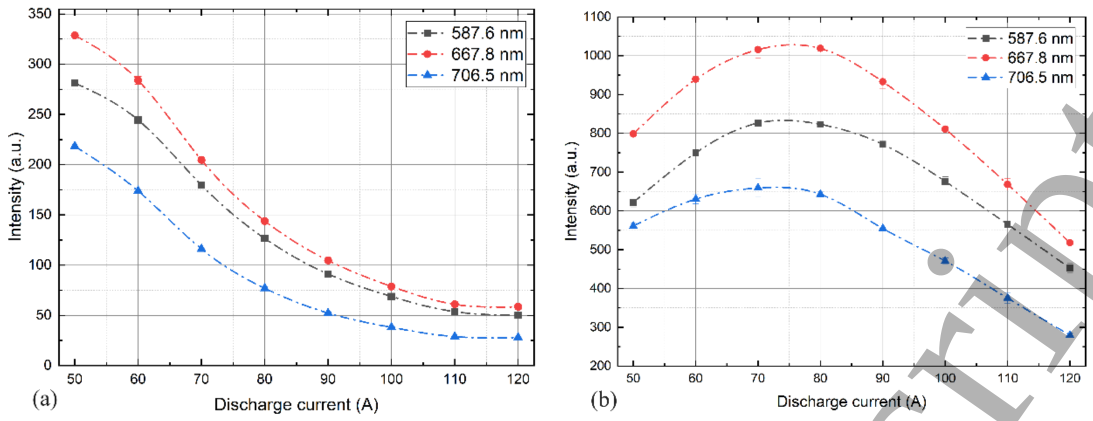

Figure 8. Intensity of He I lines (587.6 nm, 667.8 nm and 706.5 nm) as a function of discharge current with the gas flow rate of (a) 1.94 slm and (b) 3.52 slm

Plotting the intensity of He atomic lines with the wavelengths of 587.6, 667.8, and 706.5 nm against the discharge current at gas flow rates of 1.94 slm and 3.52 slm, respectively, is shown in figures 8(a) and 8(b). As discharge current increases, the intensity of these lines drops monotonically at 1.94 slm, while it initially increases and then decreases at 3.52 slm. The deceases in the lines' intensity indicate that the excited He atoms are depopulated. However, as mentioned above, the recombination reactions dominate the downstream plasma, which populates the excited He atoms yet. So, the depopulation of He^* should be caused in the cascaded arc plasma source. It is demonstrated that the increase of discharge currents can increase n_e [15, 16], which indicates that the ionization is enhanced. The excited He atoms could be consumed in the ionization processes via electron impact ionization and Penning ionization as given by

$$\begin{gathered} \mathrm{He}^* + e \rightarrow \mathrm{He}^+ + 2e \\ k_6 = 1.5\times10^{-9} T_e^{0.68} \exp\left(-24.58/T_e\right)\ \mathrm{cm^3 s^{-1}}\ ^{[36]} \end{gathered} \tag{6}$$

$$\begin{gathered} \mathrm{He}^* + \mathrm{He}^* \rightarrow \mathrm{He} + \mathrm{He}^+ + e \\ k_7 = 8.7\times10^{-10} \left(T_g/300\right)^{0.5}\ \mathrm{cm^3 s^{-1}}\ ^{[31]} \end{gathered} \tag{7}$$

Therefore, with the increase of discharge current, more He^* are ionized and the populations decrease in the plasma source. Through the recombination processes in the downstream can re-populate the He^*, the depopulation induced in the plasma source still outnumbers the population produced via recombination reactions, leading to a drop in the lines' intensity in the downstream at the gas flow rate of 1.94 slm.

At 3.92 slm, the recombination reactions are enhanced due to the high n_e [15, 16], and the population of He^* induced by the recombination reactions exceeds the depopulation caused by ionization reactions at low discharge currents. So, the lines' intensity increases at first as increasing of discharge current. When further increasing the discharge current, the ionization processes become drastic and more He^* are converted into ions. The depopulations of He^* induced by the ionization reaction surpass the populations of He^* caused by recombination reaction, leading to that the lines' intensity decreases.

3.2.3 Electron excitation temperature

For plasma with high degree of ionization ($\geq 10^{-4}$), the free electrons are solely responsible for the plasma excitation/deexcitation kinetics and the Atomic State Distribution Function (ASDF) obeys the Saha-Boltzmann distribution [37, 38]. In this case, the production and destruction of free electrons are governed by Saha balance and the excitation and deexcitation of excited levels are described by Boltzmann balance. The plasma is said to be in Local Saha Equilibrium (LSE) [37, 38]. However, in general, the electrons cannot control full ASDF but only the top excited levels. This situation is called the partial LSE (pLSE). In this case, the electron excitation temperature (T_{exc}) describing the Boltzmann distribution is equal to electron temperature (T_e).

Boltzmann plot is a popular method to determine T_{exc} which employs the relative intensity of the spectral lines using the following equation [29, 30, 39]

$$\ln\left(\frac{I_{pq}\lambda_{pq}}{A_{pq}g_p}\right) = -\frac{E_p}{k_B T_{exc}} + C \qquad (8)$$

where I_{pq} is the intensity of emitting line, λ_{pq} is the wavelength, g_p is the statistical weight of upper level p, A_{pq} is the transition probability, E_p is the energy of level p and C is a constant. Using equation (8) as a plot, where the horizontal axis is E_p and the vertical axis is $\ln\left(\frac{I_{pq}\lambda_{pq}}{A_{pq}g_p}\right)$, creates a straight line whose negative reciprocal of the slope is T_{exc}.

Table I. Spectral lines of He I and their parameters

λ_{pq} (nm)	E_p (eV)	A_{pq} (s^{-1})	g_p	Upper level	Lower level
388.86	23.0071	9.47E+06	3	1s3p $^3P_1^o$	1s2s $^3S_1$
402.62	24.0427	1.16E+07	7	1s5d $^3D_1$	1s2p $^3P_2^o$
447.15	23.7360	2.46E+07	7	1s4d $^3D_1$	1s2p $^3P_2^o$
471.31	23.5940	5.29E+06	3	1s4s $^3S_1$	1s2p $^3P_2^o$

In our work, four He lines emitted by the excited levels close to ionization state listed in Table I, are chosen to determine the T_{exc}. Figure 9 depicts the Boltzmann plot by using the four He lines. The Adj.R^2 (Adjustable Coefficient of Determination) of linear fitting is close to 0.99 which indicates that the upper levels emitting these four He I lines obeys Boltzmann distribution and the T_{exc} can be thought of as T_e.

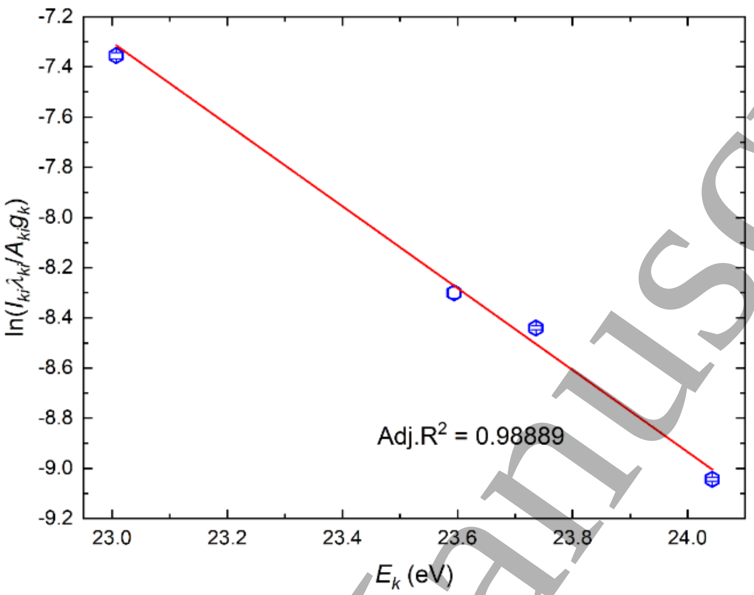

Figure 9. Boltzmann plot obtained from the He I lines selected. The discharge conditions: gas flow of 1.94 slm, discharge current of 60 A and B_{OES} = 0.67 T

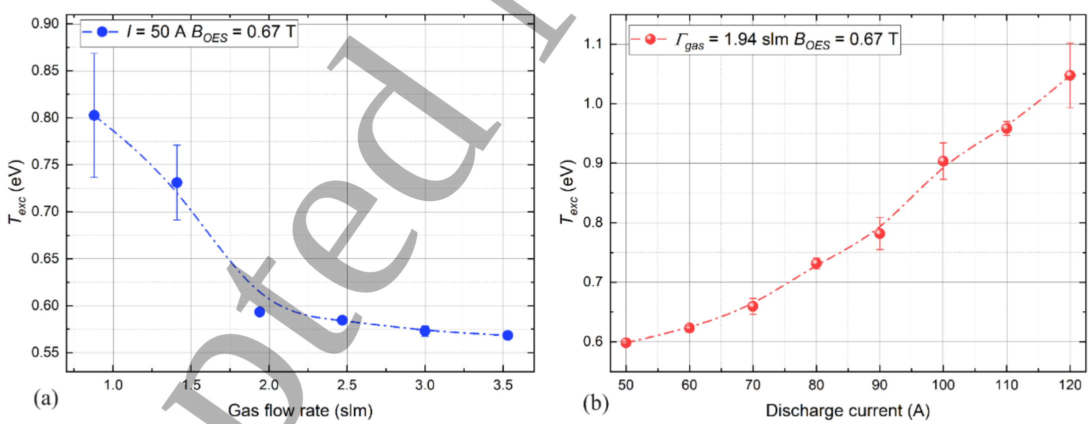

Figure 10. Electron excitation temperature as a function of (a) gas flow rate with discharge current of 50 A and B_{OES} = 0.67 T and (b) discharge current with gas flow rate of 1.94 slm and B_{OES} = 0.67 T.

In figures 10(a) and 10(b), the T_{exc} is plotted against the gas flow rate and the discharge current, respectively. In the investigated range, the T_{exc} is close to 1 eV, which is equivalent to the T_e of He plasma measured by Thomson scattering in Pilot-

PSI[27] and Magnum-PSI[24]. The T_{exc} decreases as increasing the gas flow rate and raises with the increase of the discharge current. As seen in figure 10, a rise in gas flow rate results in an increase in pressure, which may shorten the mean free path of particles in plasma. The collisions between the electrons and heavy particles become intense and the electrons loss the energy in the collision, leading to a drop in T_{exc}. As increasing the discharge current, the electric field in plasma source is enhanced as shown in figure 4(a). The electrons can obtain more energy in the enhanced electric field and T_e increase in the plasma source. Due to no external electromagnetic field in downstream plasma, the increase of T_e in upstream CAPS induces the rise in T_{exc} in downstream plasma.

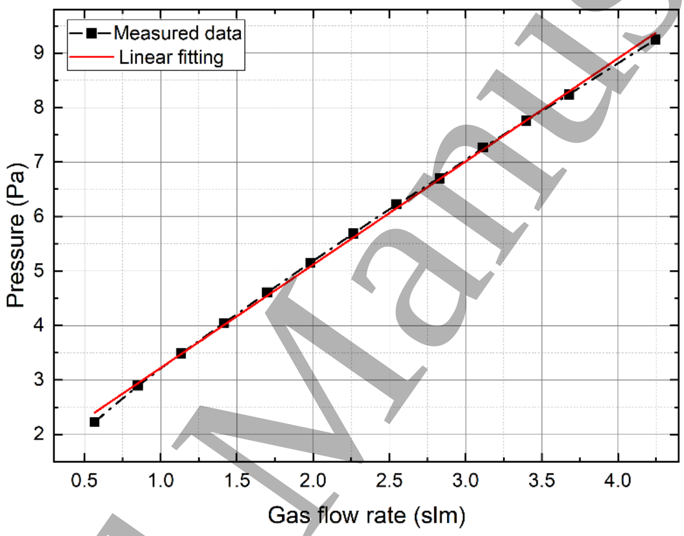

Figure 11. Correlation between pressure and gas flow rate

4. Conclusion

In summary, both the upstream and downstream He plasmas in a compact LPD are investigated by voltammetry and OES, respectively. The arc voltage, behaviors of emission lines and T_{exc} in the He plasma are studied.

1. Based on the equation $E = j/\sigma$, the *V-I* curve has a positive slope because of the increase in current density brought on by the rise in discharge current. At the low gas flow, the increase of gas flow rate could broaden arc column, leading to a drop in the voltage whilst the cool gas reduces the plasma temperature and σ decreases so that the voltage turns to increase at large gas flow rate. In addition, a local reverse electric field is observed between the two cascaded plates close to the cathode.

2. The intensity of three typical He atomic lines (587.6 nm, 667.8 nm, and 706.5

nm) increase with the gas flow rate because recombination reactions can populate the upper levels. The monotonic decreases in these lines' intensity at the gas flow rate of 1.94 slm are observed as increasing the discharge current, which is ascribed to the depopulation of upper levels in the ionization processes in plasma source. In contrast, with the increase of discharge current at gas flow rate of 3.52 slm, these lines exhibit an initial increase in intensity followed by a subsequent reduction. The upper levels should be populated by the recombination reactions at small current, whereas at large current the ionization processes become drastic, causing the depopulation of upper levels and a decrease in line's intensity.

3. The electron excitation temperature is calculated by Boltzmann plot on the assumption that the top levels of He atoms are in pLSE. Increased pressure from rising gas flow rates causes drastic collisions between electrons and heavy particles. In the collision, the electrons lose energy and T_{exc} falls. More power is input into the plasma source as the discharge current increases, and the electron is heated by Ohm heating. Thus, the electron temperature in plasma source rise, which results in an increase of electron temperature in downstream plasma, namely T_{exc} increases.

Acknowledgement

This work was supported by the National Natural Science Foundation of China (Nos. 12105317) and Comprehensive Research Facility for Fusion Technology Program of China (No. 2018-000052-73-01-001228).

Data availability statement

All data that support the findings of this study are included within the article (and any supplementary files).

Reference

[1] Linsmeier C, Unterberg B, Coenen J W, *et al*. 2017, Material testing facilities and programs for plasma-facing component testing [J]. *Nucl Fusion*, 57(9): 092012.

[2] van Rooij G J, Veremiyenko V P, Goedheer W J, *et al*. 2007, Extreme hydrogen plasma densities achieved in a linear plasma generator [J]. *Appl Phys Lett*, 90(12): 121501.

[3] van Eck H J N, Akkermans G R A, Alonso van der Westen S, *et al*. 2019, High-fluence and high-flux performance characteristics of the superconducting Magnum-PSI linear plasma facility [J]. *Fusion Eng Des*, 142: 26-32.

[4] Kakati M, Sarmah T, Aomoa N, *et al*. 2019, Design, development and recent experiments of

the CIMPLE-PSI device [J]. *Nucl Fusion*, 59(11): 112008.

[5] Caneses J F, Spong D A, Lau C, *et al*. 2020, Effect of magnetic field ripple on parallel electron transport during microwave plasma heating in the Proto-MPEX linear plasma device [J]. *Plasma Phys Control Fusion*, 62(4): 045010.

[6] van de Pol M J, Alonso van der Westen S, Aussems D U B, *et al*. 2018, Operational characteristics of the superconducting high flux plasma generator Magnum-PSI [J]. *Fusion Eng Des*, 136: 597-601.

[7] de Groot B, Al R S, Engeln R, *et al*. 2007, Extreme hydrogen plasma fluxes at Pilot-PSI enter the ITER divertor regime [J]. *Fusion Eng Des*, 82(15-24): 1861-1865.

[8] Rapp J, Koppers W R, van Eck H J N, *et al*. 2010, Construction of the plasma-wall experiment Magnum-PSI [J]. *Fusion Eng Des*, 85(7-9): 1455-1459.

[9] Ohno N, Nishijima D, Takamura T, *et al*. 2001, Static and dynamic behavior of plasma detachment in the divertor simulatore experiment NAGDIS-II [J]. *Nucl Fusion*, 41(8): 1055-1065.

[10] Hirooka Y, Conn R W, Sketchley T, *et al*. 1990, A new plasma-surface interactions research facility: PISCES-B and first materials erosion experiments on bulk-boronized graphite [J]. *J Vac Sci Technol A*, 8(3): 1790-1797.

[11] Kreter A, Brandt C, Huber A, *et al*. 2017, Linear plasma device PSI-2 for plasma-material interaction studies [J]. *Fusion Sci Technol*, 68(1): 8-14.

[12] Zhou H-S, Yuan X-G, Li B, *et al*. 2021, A new high flux plasma source testing platform for the CRAFT project [J]. *J Fusion Energ*, 39(6): 355-360.

[13] Yuan X, Zhou H, Liu H, *et al*. 2021, Particle flux characteristics of a compact high-field cascaded arc plasma device [J]. *Plasma Sci Technol*, 23(11): 115402.

[14] Engeln R, Klarenaar B, Guaitella O. 2020, Foundations of optical diagnostics in low-temperature plasmas [J]. *Plasma Sources Sci Technol*, 29(6): 063001.

[15] Ma X, Cao X, Han L, *et al*. 2018, Characterization of high flux magnetized helium plasma in SCU-PSI linear device [J]. *Plasma Sci Technol*, 20(2): 025104.

[16] Wang Y, Zhou L, Shi J, *et al*. 2024, Observation of the low electron density and electron temperature in an unmagnetized cascaded arc helium plasma by laser Thomson scattering approach [J]. *Plasma Phys Control Fusion*, 66(4): 045014.

[17] Vijvers W A J, van Gils C A J, Goedheer W J, *et al*. 2008, Optimization of the output and efficiency of a high power cascaded arc hydrogen plasma source [J]. *Phys Plasmas*, 15: 093507.

[18] Li G, Pan W, Meng X, *et al*. 2005, Application of similarity theory to the characterization of non-transferred laminar plasma jet generation [J]. *Plasma Sources Sci Technol*, 14(2): 219-225.

[19] Ikoma N, Miyake Y, Takahashi M, *et al*. 2020, Characteristics of plasma window with various channel diameters for accelerator applications [J]. *Rev Sci Instrum*, 91(5): 053503.

[20] Bora B, Aomoa N, Kakati M. 2010, Characteristics and temperature measurement of a non-transferred csacaded DC plasma torch [J]. *Plasma Sci Technol*, 12: 181-187.

[21] Paingankar A M, Das A K, Shirodkar V S, *et al*. 1999, Prediction of electrical characteristics of a non-transferred arc plasma torch using principles of dynamic similarity [J]. *Plasma Sources Sci Technol*, 8: 100-109.

[22] Valinius V, Kruinskaite V, Valatkeviius P, *et al*. 2004, Electric and thermal characteristics of the linear, sectional dc plasma generator [J]. *Plasma Sources Sci Technol*, 13(2): 199-206.

[23] Das A K, Sreekumar K P, Venkatramani N. 1993, DC plasma torch voltage and current charactersitics through heat balance measurements [J]. *Plasma Sources Sci Technol*, 3: 108-113.

[24] Kajita S, Iwai S, Tanaka H, *et al*. 2022, Use of machine learning for a helium line intensity ratio method in Magnum-PSI [J]. *Nucl Mater Energy*, 33: 101281.

[25] Ma X, Cao X, Cao Z, *et al*. 2017, Characteristics of helium plasma produced in cascade arc discharge [J]. *Nuclear Fusion and Plasma Physics*, 37(3): 267-273.

[26] Kajita S, Akkermans G, Fujii K, *et al*. 2020, Emission spectroscopy of He lines in high-density plasmas in Magnum-PSI [J]. *AIP Adv*, 10(2): 025225.

[27] Hayashi Y, Ješko K, van der Meiden H J, *et al*. 2016, Plasma detachment study of high density helium plasmas in the Pilot-PSI device [J]. *Nucl Fusion*, 56(12): 126006.

[28] Meulenbroeks R F, van Beek A J, van Helvoort A J, *et al*. 1994, Argon-hydrogen plasma jet investigated by active and passive spectroscopic means [J]. *Phys Rev E*, 49(5): 4397-4406.

[29] Wang Y, Li C, Shi J, *et al*. 2017, Measurement of electron density and electron temperature of a cascaded arc plasma using laser Thomson scattering compared to an optical emission spectroscopic approach [J]. *Plasma Sci Technol*, 19(11): 115403.

[30] Wang Y, Shi J, Li C, *et al*. 2019, Comparative study of electron temperature in cascaded arc Ar/N_2 plasma using laser Thomson scattering combined optical emission spectroscopy approach [J]. *AIP Adv*, 9: 125307.

[31] Liu D X, Bruggeman P, Iza F, *et al*. 2010, Global model of low-temperature atmospheric-pressure He + H_2O plasmas [J]. *Plasma Sources Sci Technol*, 19(2): 025018.

[32] Nersisyan G, Graham W G. 2004, Characterization of a dielectric barrier discharge operating in an open reactor with flowing helium [J]. *Plasma Sources Sci Technol*, 13(4): 582-587.

[33] Anderson C, Hur M, Zhang P, *et al*. 2004, Two-dimensional space-time-resolved emission spectroscopy on atmospheric pressure glows in helium with impurities [J]. *J Appl Phys*, 96(4): 1835-1839.

[34] Ha C S, Choi J Y, Kim D H, *et al*. 2009, Properties of dielectric-barrier-free atmospheric pressure microplasma driven by submicrosecond dc pulse voltage [J]. *Appl Phys Lett*, 95(6): 061502.

[35] Golubovskii Y B, Maiorov V A, Behnke J, *et al*. 2003, Modelling of the homogeneous barrier discharge in helium at atmospheric pressure [J]. *J Phys D-Appl Phys*, 36: 39-49.

[36] Xiaohui Y, Raja L L. 2003, Computational study of capacitively coupled high-pressure glow discharges in helium [J]. *IEEE Trans Plasma Sci*, 31(4): 495-503.

[37] Sáinz A, García M C. 2008, Spectroscopic characterization of a neon surface-wave sustained (2.45 GHz) discharge at atmospheric pressure [J]. *Spectroc Acta Pt B-Atom Spectr*, 63(9): 948-956.

[38] Rincón R, Muñoz J, Calzada M D. 2015, Departure from Local Thermodynamic Equilibrium in argon plasmas sustained in a Torche à Injection Axiale sur Guide d'Ondes [J]. *Spectroc Acta Pt B-Atom Spectr*, 103-104: 14-23.

[39] Li C, Zhang J, Yao Z, *et al*. 2013, Diagnosis of electron, vibrational and rotational temperatures in an Ar/N_2 shock plasma jet produced by a low pressure dc cascade arc discharge [J]. *Plasma Sci Technol*, 15(9): 875-880.